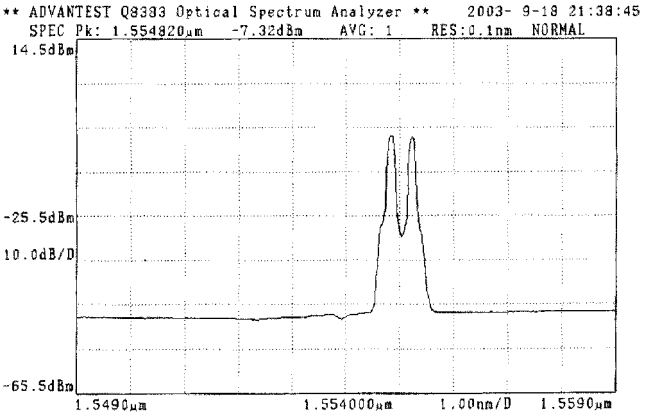

Figure 3 Output spectrum of the dual-wavelength EDFL when the axial strain is 818 $\mu\varepsilon$ and the screwed angle is 50°

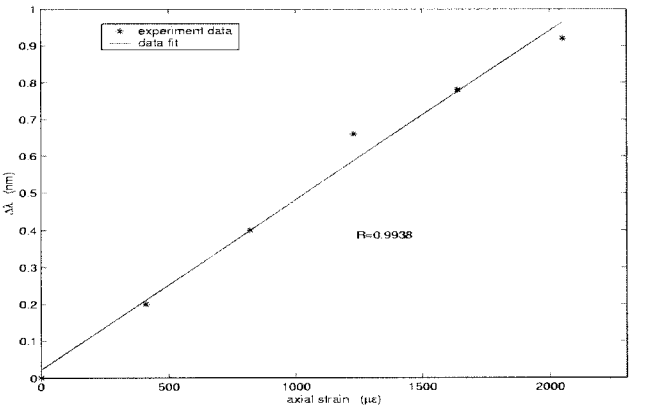

Figure 5 Dependence of the lasing wavelength shift upon the axial strain

produced, or the same thresholds for both modes can be obtained, which results in the third state.

By using the tuning scheme to apply axial and lateral strain on the FBG, we can change the wavelengths of the dual-wavelength laser. Figure 3 shows the output spectrum of the EDFL when the axial strain is 818 $\mu\varepsilon$ (according to the translation stage's displacement of 0.1 mm) and the screw angle is 50°. The dual lasing wavelengths are 1554.44 and 1554.84 nm, respectively.

Figure 4 shows the dependence of the wavelength spacing upon the lateral strain when the axial strain is zero and Figure 5 shows the wavelength shift with respect to the axial strain when the lateral strain is zero. Linear responses were observed in both figures. Considering the mechanical properties of glass fiber, the wavelength shift can not exceed $\sim$ 2 nm using the axial-strain tuning method.

4. CONCLUSION

In conclusion, we have demonstrated a tunable, stable dual-wavelength EDFL at room temperature with only a single-mode FBG applied with lateral strain. Adjusting a PC in the cavity allows us to achieve either single- or dual-wavelength laser outputs. Two lasing wavelengths of this simple and low-cost laser can be tuned continuously.

ACKNOWLEDGMENTS

This work is supported by the Tianjin Natural Science Foundation project, multiwavelength optical fiber laser in DWDM communication systems, under grant no. 013601811, and the startup Foundation of Scientific Research provided by the Personnel Department of Nankai University, P.R. China.

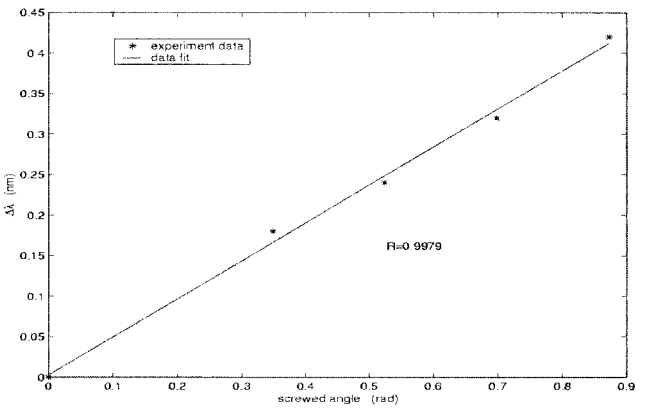

Figure 4 Dependence of the lasing wavelength spacing upon the screwed angle

REFERENCES

1. H.L. An, X.Z. Lin, E.Y.B. Pun, and H.D. Liu, Multi-wavelength operation of an erbium-doped fiber ring laser using a dual-pass Mach–Zehnder comb filter, Opt Commun 169 (1999), 159–165.
2. X.P. Dong, S.P. Li, K.S. Chiang, M.N. Ng, and B.C.B. Chu, Multi-wavelength erbium-doped fibre laser based on a high-birefringence fibre loop mirror, Electron Lett 36 (2000), 1609–1610.
3. O. Graydon, W.H. Loh, R.I. Laming, and L. Dong, Triple-frequency operation of an Er-doped twincore fiber loop laser, IEEE Photon Technol Lett 8 (1996), 63–65.
4. G. Das and J.W.Y. Lit, L-band multiwavelength fiber laser using an elliptical fiber, IEEE Photon Technol Lett 14 (2002), 606–608.
5. D.H. Zhao, X.W. Shu, W. Zhang, Y.C. Lai, L. Zhang, and I. Bennion, Stable dual-wavelength oscillation of an erbium-doped fiber ring laser at room temperature, Proc SPIE 4914 (2002), 488–492.
6. V.J. Mazurczyk and J.L. Zyskind, Polarization dependent gain in erbium-doped fiber amplifiers, IEEE Photon Technol Lett 6 (1994), 616–618.
7. R. Gafsi and M.A. El-Sherif, Analysis of induced birefringence effects on fiber Bragg gratings, Opt Fiber Technol 6 (2000), 299–323.
8. S.P. Reilly, S.W. James and R.P. Tatam, Tunable and switchable dual wavelength lasers using optical fiber Bragg grating external cavities, Electron Lett 38 (2002), 1033–1034.

© 2004 Wiley Periodicals, Inc.

DESIGN AND ANALYSES OF COMPACT BENT-TAPERED WAVEGUIDES USING GUIDED-WAVE LENS SETS

Chun-Wen Chang and Wen-Feng Hsieh
Institute of Electro-Optical Engineering
National Chiao Tung University
Hsinchu, Taiwan 30050, ROC

Received 19 January 2004

ABSTRACT: *We propose compact bent-tapered waveguides using guided-wave lens sets, which are constructed by disposing lens-shaped waveguide regions in planar tapered waveguides. Two applications of the abruptly bent tapered waveguide and the Z-bend tapered waveguide demonstrate high transmittances of 91% and 86% with bent and tapered*

angles of 10°. © 2004 Wiley Periodicals, Inc. Microwave Opt Technol Lett 42: 324–328, 2004; Published online in Wiley InterScience (www.interscience.wiley.com). DOI 10.1002/mop.20292

Key words: *guided-wave lens sets; tapered waveguides; bent waveguides*

1. INTRODUCTION

Low-index-contrast silica waveguides, offering low propagation losses and high-efficiency coupling with a single-mode fiber, have been utilized in a number of optical-communication devices. In such devices, waveguide tapers and waveguide bends are frequently used to interconnect integrated photonic devices with different cross sections and directions. However, the tapered angles and the bent angles should be less than 2° to prevent serious radiation losses in the low-index-contrast waveguides [1]. These limitations are obstacles to realizing high-density photonic integrated circuits (PICs), and thus prevent the production cost from being reduced. Hence, shorter bent-tapered waveguides, which combine the functions of waveguide bends and tapers, are desired.

Much attention has been paid to the design and analyses of waveguide tapers [2, 3] and waveguide bends [4–6]. Marcatili [7] presented a design procedure, based on the scalar wave equation, for developing lossless curved-axes tapered waveguides. Although these ideal waveguide structures cannot be readily implemented in practical applications, they do provide good insight into the mechanism of the operation of curved-axis waveguides. Using the guided-wave lenses [8], we have analogized guided-wave telescopes in order to design planar tapered waveguides [3], in which an input mode can only be converted along a straight axis. In this paper, we extend the application of guided-wave telescopes to bent-tapered waveguides by introducing lateral displacements between the axes of the optical elements in the guided-wave telescope structures. The function of the laterally shifted lens sets can be regarded as being equivalent to that of a combination of planar prisms and mode converters.

The methods of designing the proposed bent-tapered waveguides are based on a combination of the paraxial transfer-function method (TFM) and ray optics with guided-wave parameters. Two bent-tapered waveguides, the abrupt-bent tapered (ABT) waveguide and the Z-bend tapered (ZBT) waveguide, are demonstrated to elucidate the functions of the proposed schemes. This investigation applies the beam-propagation method (BPM) to calculate the transmission efficiency of the proposed bent-tapered waveguides. Meanwhile, reflection and scattering from the boundaries of waveguide lenses are investigated using the finite-difference time-domain (FDTD) method. The transmission spectra of the bent-tapered devices are discussed to verify the applicability of the proposed devices in wide-bandwidth optical-fiber communication systems.

2. THEORY

Figure 1(a) depicts a tapered waveguide with a guided-wave telescope structure [3]. Lens A with a positive focal length f_a and lens B with a negative focal length f_b are employed to transform a broad plane-wave beam into a narrower beam, such that the Galilean condition, $\Delta z = f_a - |f_b|$, is fulfilled, where Δz is the tapered length. Figure 1(b) presents the proposed ABT waveguide. The guided-wave lens set in the ABT waveguide is the same as that shown in Figure 1(a), but with a lateral shift between the two lenses. Introducing the lateral shift between the guided-wave lenses bends the waveguide beam to the output channel of the ABT with an angle θ, which can be predicted from the paraxial TFM. The paraxial transfer function of these two lenses in Figure 1(b), using the thin-lens approximation, can be expressed as

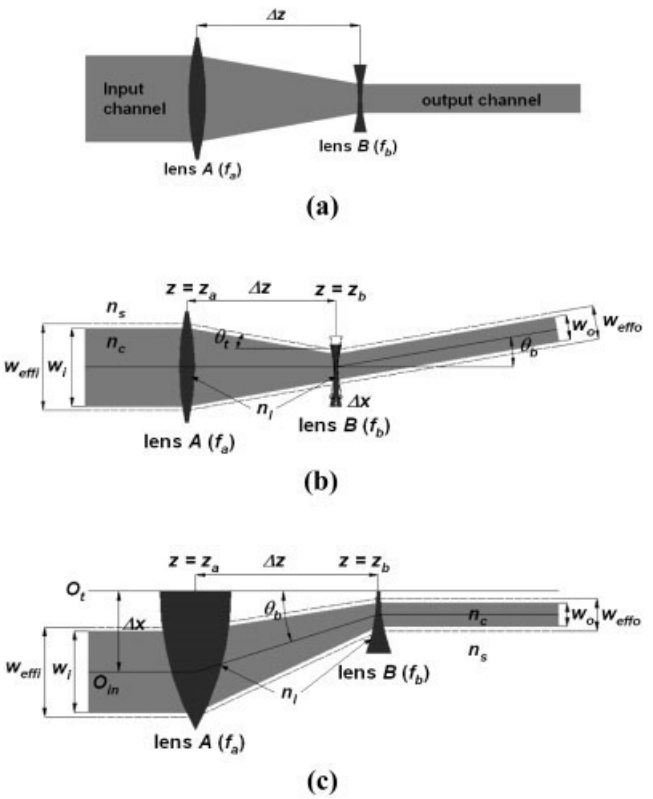

Figure 1 Geometry and basic operation principle of the (a) conventional guided-wave lens tapered waveguides, (b) proposed abrupt-bent tapered waveguides, and (c) proposed Z-bend tapered waveguides

$$\tilde{t}_a = \exp\left(-j\frac{\pi x^2}{\lambda f_a}\right) \text{ and } \tilde{t}_b = \exp\left(+j\frac{\pi(x-\Delta x)^2}{\lambda f_b}\right), \quad (1)$$

where $\tilde{t}_a$ represents the transfer function of lens A and $\tilde{t}_b$ is that of lens B, which is laterally shifted by Δx relative to lens A, and λ is the wavelength. The negative and the positive signs in Eq. (1) are associated with a converging lens and a diverging lens, respectively. The input waveguide presented in Figure 1(b) is coaxial with lens A. After leaving the first lens, the planar wavefront is immediately altered by lens A and the complex amplitude $\tilde{U}$ of the beam becomes

$$\tilde{U}(x,z=z_a^+) = E(x)\exp\left(-j\frac{\pi x^2}{\lambda f_a}\right), \quad (2)$$

where $E(x)$ represents the initial distribution of the electric field of the beam. It is a spherical wave that converges to the focus of lens A. After the beam has traveled a distance of Δz to reach lens B, the beam diameter is reduced and the radii of the curvatures of the wavefronts exactly match the curvature of lens B. Immediately, behind lens B, the amplitude $\tilde{U}$ of the propagating wave is given by

$$\tilde{U}(x,z=z_b^+) = E(x)\frac{f_a}{f_b}\exp\left(j\frac{\pi\Delta x^2}{\lambda f_b}\right)\exp\left(-j\frac{2\pi\Delta x}{\lambda f_b}x\right). \quad (3)$$

The first phase term of Eq. (3) is a constant, whereas the second term represents a linear phase shift across the aperture of the lens and is proportional to the lateral shift Δx. Consequently, the complex amplitude specified by Eq. (3) reveals that the laterally

shifted telescope structure not only serves as a plane-wave beam-shaping system, but also as a refractive prism that deflects the incoming plane-wave beam to an angle, given by

$$\theta_b = -\arctan\left(\frac{\Delta x}{f_b}\right). \tag{4}$$

The negative sign indicates that the deflection takes place in the direction opposite to the lateral shift.

Similarly, the parameters used to design the ZBT waveguides can also be obtained using the TFM. The ZBT waveguide is composed of a truncated telescope and a bent-tapered waveguide, as shown in Figure 1(c), where O_t and O_{in}, which are separated by Δx, are axes of the guided-wave telescope and the input waveguide, respectively. Consider a plane-wave beam incident onto lens A with a focal length f_a; the transmitted amplitude of the collimated beam immediately after lens A is given by

$$\tilde{U}(x,z=z_a^+) = E(x)\exp\left(-j\frac{\pi\Delta x^2}{\lambda f_a}\right)\exp\left(-j\frac{\pi x^2}{\lambda f_a}\right)\exp\left(j\frac{2\pi\Delta x}{\lambda f_a}\right). \tag{5}$$

The second phase term of Eq. (5) specifies that the transmitted waves converge to the focus of lens A in Figure 1(c). The third exponential term shows that the converging beam is deflected through the following angle:

$$\theta_b = \arctan\left(\frac{\Delta x}{f_a}\right). \tag{6}$$

Following multiplication by the transfer function of lens B, the outgoing beam is converted into a planar beam and then becomes parallel to the input channel.

3. DESIGN AND CALCULATIONS

3.1. Abrupt-Bent Tapered Waveguides

The core and cladding of the ABT waveguide with a bent angle of θ_b, as shown in Figure 1(b), have refractive indices $n_c = 1.504$ and $n_s = 1.5$, respectively. In Figure 1(b), the straight waveguide with width $w_i = 27$ μm is excited by the fundamental transverse electric (TE) mode of wavelength $\lambda = 1.5$ μm and serves as the input channel of the tapered waveguide. Accordingly, the propagation constant β and the effective waveguide width w_{effi} of the input waveguide can be determined. The input waveguide is connected to the output waveguide via a tapered region with a tapered angle θ_t. In these analyses, the width of the output waveguide is assumed to be 9 μm; a tapered angle of $\theta_t = 10°$ and bent angles of $\theta_b = 0 - 10°$ are used. The focal length f_a of lens A is given by

$$\sin(\theta_t) = \frac{w_{effi}/2}{\sqrt{(w_{effi}/2)^2 + f_a^2}}, \tag{7}$$

when the tapered angle θ_t and the effective waveguide width w_{effi} are specified. The radii of the curvatures of the lens set, r_1 and r_2, can be calculated using Lensmaker's formula:

$$\frac{n_m}{f} = (n_l - n_m)\left(\frac{1}{r_1} - \frac{1}{r_2}\right), \tag{8}$$

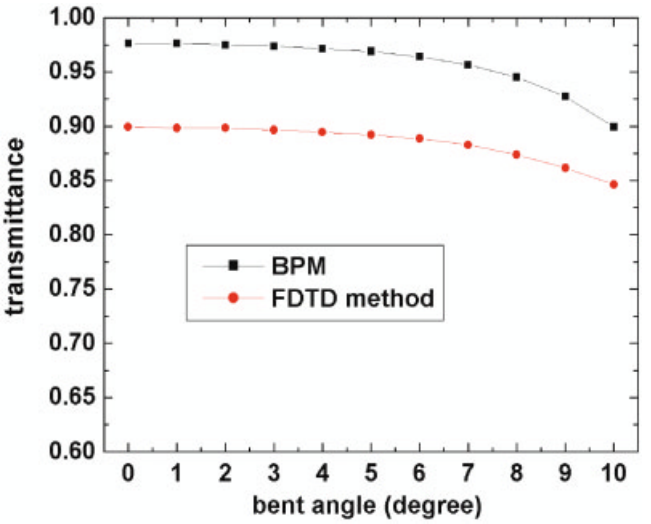

Figure 2 Transmittance vs. the bent angles for the ABT waveguide using the BPM and FDTD methods. [Color figure can be viewed in the online issue, which is available at www.interscience.wiley.com.]

where f is the focal length of the lens, and n_l and n_m are the refractive indices of the lens and the ambient media, respectively. In this study, the guided-wave parameters, which are the effective refractive indices of the straight waveguides n_{eff}, are taken to be n_m and the refractive indices of the lenses are assumed to be $n_l = 2.0$ (Si_3N_4).

The grid size in the BPM calculation is 1/20 of the wavelength, and transparent boundary conditions are imposed to prevent reflection of the radiation waves at the boundaries of the calculation domain. The transmittance η is determined from the overlap integral between the field calculated at the output position and the mode field of the output channel. Figure 2 shows the transmittance versus the bent angles of the ABT with $\theta_t = 10°$. As indicated, the excess losses are less than 0.46 dB ($\eta = 91\%$) when the bent and tapered angles are both 10°. In Figure 3(a), the field distribution along the ABT waveguide with $\theta_b = 10°$ shows that the propagating waves were tapered and bent with low radiation losses, performing low-loss mode conversions and high-efficiency transmission in the bent-tapered structure. Therefore, the guided-wave lens sets can considerably reduce the dimensions and the excess losses of the ABT waveguides when the bent angles are from 0° to 10°.

3.2. Z-bend Tapered Waveguides

In Figure 1(c), the ZBT waveguide constructed using the truncated guided-wave lens set provides a lateral offset in the waveguide path in order to enable the connection of two parallel noncollinear photonic devices with different cross sections. The parameters of the input and the output straight waveguides are the same as those of the ABT waveguide analyzed above. The truncated lens A, which has a focal length $f_a = 159.5$ μm, is separated from the truncated lens B by a distance $\Delta z = 100.7$ μm. The aperture width of the truncated guided-wave lens sets should be sufficiently wide to cover the effective waveguide width of the input and output channels.

Figure 4 shows the transmittance of the ZBT waveguide against the bent angles. The excess losses are 0.65 dB ($\eta = 86\%$) when the bent angle is as large as 10°. Figure 5(a) plots the field intensity distribution of the ZBT waveguide with a bent angle of $\theta_b = 10°$. The propagating waves in the input straight waveguide are tapered

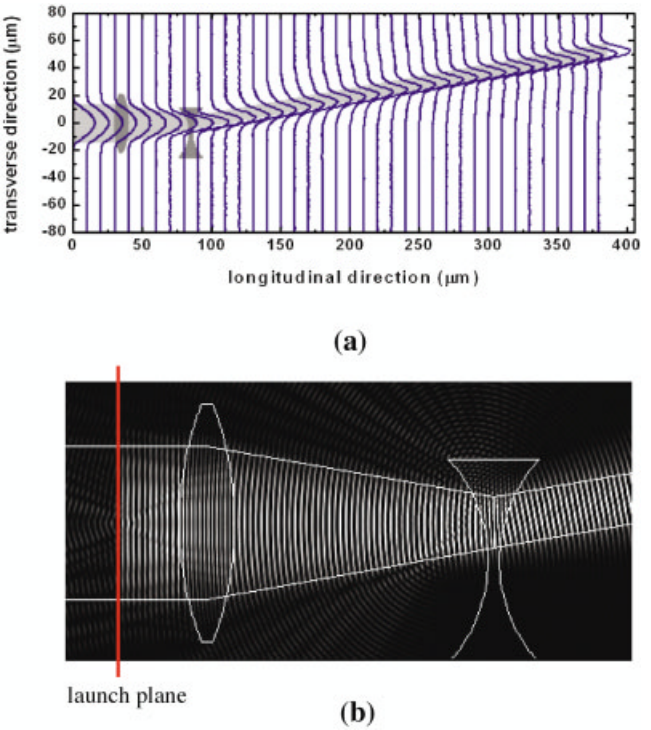

Figure 3 Plots of (a) the optical field intensity and (b) the electric field intensity of the ABT waveguides. [Color figure can be viewed in the online issue, which is available at www.interscience.wiley.com.]

and bent properly by the lens sets. Therefore, the proposed ZBT waveguides providing low-loss bends and tapers of the propagating waves are appropriate for realizing the compact transverse offsets and cross section tapers in PICs.

3.3. Reflections and Scattering from the Waveguide-lens Boundaries

Since the waveguide lenses are made of material with higher indices (Si_3N_4, $n = 2.0$), reflection and scattering should occur at the waveguide-lens boundaries. However, the single-directional BPM is not suitable for investigating reflections. This study employs the FDTD method, which directly integrates Maxwell's equations with respect to time in order to calculate the transmittance and reflectance, as presented in Figures 2 and 4 for the ABT and ZBT waveguides, respectively. From Figures 2 and 4, the excess losses caused by reflection and scattering from the lens boundaries are between 0.17 dB and 0.4 dB, which depend on the bent angles and the structures of the tapered waveguides. The respective electric-field distributions of the ABT and the ZBT waveguides shown in Figures 3(b) and 5(b) reveal that the cross sections of the guided modes were effectively converted due to the curved-wavefront effect caused by the waveguide lenses. The introduced lateral shifts yielded highly efficient bends and tapers. Furthermore, most of the reflected waves radiated out of the waveguide region and did not propagate backward along the input waveguide since the curved boundaries caused them either to diverge or to converge. The reflectances calculated by the FDTD method are both less than −40 dB for the ABT and ZBT waveguides, which meet the requirements of digital-communication systems.

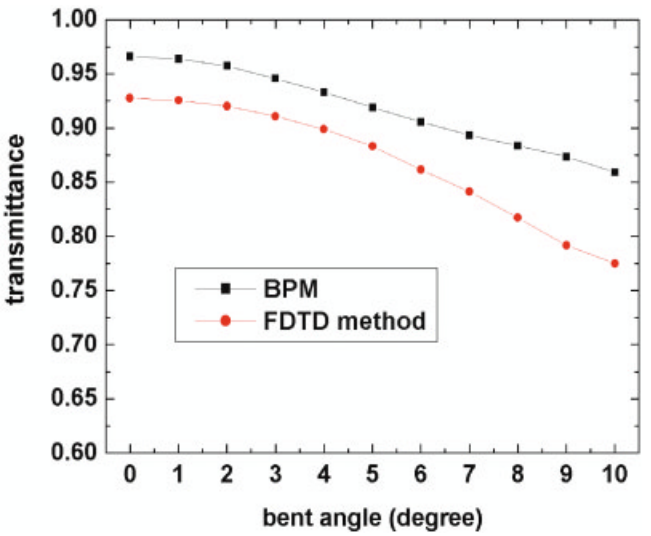

Figure 4 Transmittance vs. the bent angles for the ZBT waveguide using the BPM and FDTD methods. [Color figure can be viewed in the online issue, which is available at www.interscience.wiley.com.]

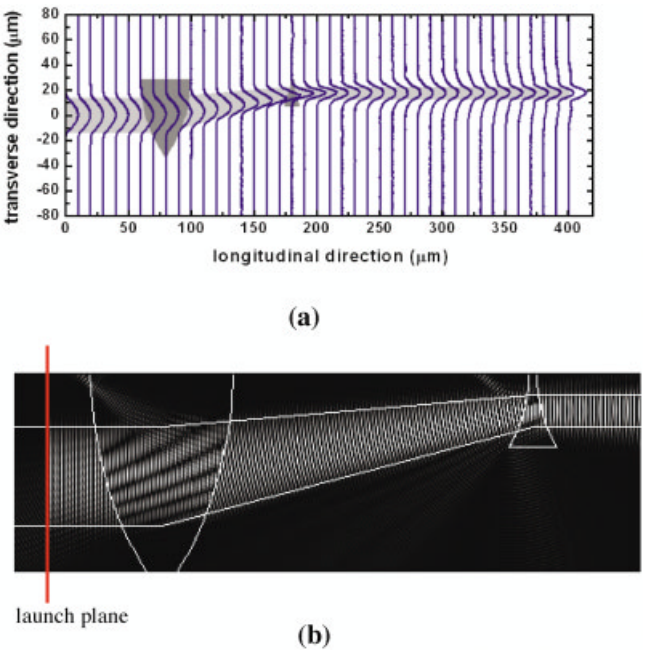

Figure 5 Plots of (a) the optical field intensity and (b) the electric field intensity of the ZBT waveguides. [Color figure can be viewed in the online issue, which is available at www.interscience.wiley.com.]

3.4. Wavelength Responses

The spectral responses of the proposed bent-tapered waveguides were analyzed as plotted in Figure 6 to verify the applicability of the proposed devices in optical-fiber communication systems. In spite of the dispersion of the guided-wave parameters used in the design, the transmittances of the proposed devices with tapered and bent angles of 10° are uniform across the spectral range of 1400 to 1600 nm. The uniformity, which was defined as the maximum power divided by the minimum power, was 0.026 dB for the ABT waveguide and 0.058 dB for the ZBT waveguide, respectively. Accordingly, the proposed bent-tapered waveguides with uniform spectral responses are very useful in wide-bandwidth optical-fiber communication applications.

4. CONCLUSION

We have demonstrated two types of bent-tapered waveguides with low excess losses and wide bandwidths using guided-wave lens

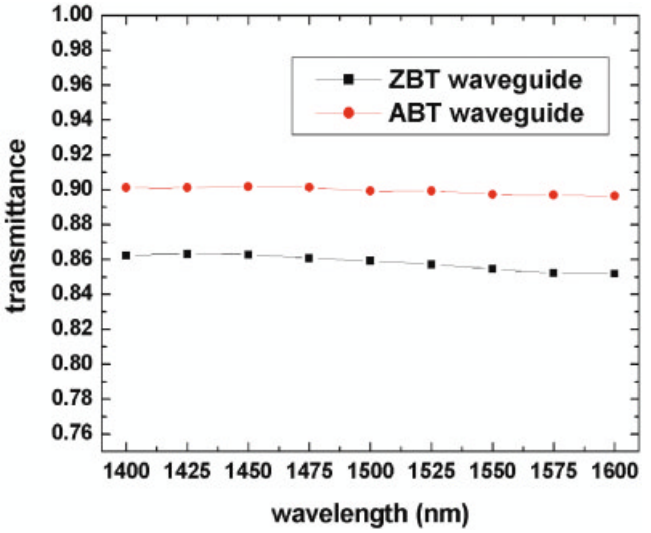

Figure 6 Wavelength responses of the ABT and ZBT waveguides. [Color figure can be viewed in the online issue, which is available at www.interscience.wiley.com.]

sets. The procedures for designing the proposed bent-tapered waveguides are derived from the paraxial TFM and ray optics with guided-wave parameters. The results of the BPM calculation reveal that the excess losses of the ABT and ZBT waveguides are less than 0.46 and 0.65 dB, respectively, when the bent and tapered angles are 10°. Consequently, the proposed method is very appropriate for designing high-packing-density PICs in wide-bandwidth optical-fiber communication systems.

ACKNOWLEDGMENTS

This work was partially supported by the National Science Council of Taiwan under grant no. NSC-92-2112-M009-040, and partially supported by the Neostones Microfabrication Corporation.

REFERENCES

1. H.B. Lin, J.Y. Su, P.K. Wei, and W.S. Wang, Design and application of very low-loss abrupt bends in optical waveguides, IEEE J Quantum Electron 30 (1994), 2827–2835.
2. K. Kasaya, O. Mitomi, M. Naganuma, Y. Kondo, and Y. Noguchi, A simple laterally tapered waveguide for low-loss coupling to single-mode fibers, IEEE Photon Technol Lett 5 (1993), 345–347.
3. C.W. Chang, M.L. Wu, and W.F. Hsieh, Design of low-loss tapered waveguides using the telescope structure compensation, IEEE Photon Technol Lett 15 (2003), 1378–1380.
4. M. Popovic, K. Wada, S. Akiyama, H.A. Haus, and J. Michel, Air trenches for sharp silica waveguide bends, J Lightwave Technol 20 (2002), 1762–1772.
5. J.J. Su and W.S. Wang, Novel coherently coupled multisectional bending optical waveguide, IEEE Photon Technol Lett 14 (2002), 1112–1114.
6. A.M. Shajakhan and S. Aditya, Slope-matched S-bends for inclined integrated-optic waveguides, Microwave Opt Technol Lett 24 (2000), 267–271.
7. E.A.J. Marcatili, Dielectric tapes with curved axes and no loss, IEEE J Quantum Electron 21 (1985), 307–314.
8. T.J. Su and C.C. Lee, An embedded waveguide lens with anti-reflection layer, IEEE Photon Technol Lett 6 (1994), 89–91.

© 2004 Wiley Periodicals, Inc.

DESIGN MODEL FOR BROADSIDE-COUPLED SUSPENDED SUBSTRATE STRIPLINE FOR MICROWAVE AND MILLIMETER-WAVE APPLICATIONS

Raj Kumar
Institute of Armament Technology
PUNE–411 025, India

Received 3 February 2004

ABSTRACT: *Simple closed-form expressions for the analysis of broadside coupled suspended substrate stripline is presented. The expressions are valid over a wide range of structural parameters and dielectric constants. The validity range of this expression for structural parameters is* $1.0 \leq \varepsilon_r \leq 30.0$ *(dielectric constant),* $0.2 \leq W/b \leq 10.0$ *(strip width), and* $d/b \leq 0.5$ *(substrate thickness). The average accuracies of the present expressions are* $<0.8\%$ *and* $<0.6\%$ *for even- and odd-mode impedances, respectively. The maximum deviation is* $\pm 1.25\%$ *and* $\pm 1.16\%$ *for even- and odd-mode impedances with respect to the reference values. This closed-form model is useful for the interactive CAD analysis of microwave and millimeter-wave circuit.* © 2004 Wiley Periodicals, Inc. Microwave Opt Technol Lett 42: 328–331, 2004; Published online in Wiley InterScience (www.interscience.wiley.com). DOI 10.1002/mop.20293

Key words: *suspended substrate; broadside coupled stripline; broadside coupled suspended substrate stripline*

1. INTRODUCTION

The suspended substrate striplinelike transmission line has some attractive features, such as low attenuation and large tolerance of fabrication. The suspended substrate structure has been extensively used in microwave active and passive circuits, such as mixers, oscillators, multipliers, couplers, and filters.

Coupled-line structures are utilized extensively to form microwave circuits. The edge-coupled line structure is not suitable for tight coupling (3 dB) because the gap between strip lines is difficult too realize. The broadside-coupled stripline [1] is particularly useful in circuits where tight coupling is required, whereas broadside-coupled suspended substrate is suitable for tight coupling as well as low attenuation for microwave and millimeter-wave circuits.

A number of numerical approaches for the analysis of the broadside-coupled line structure have been published in literature [2–6], but all of these approaches required extensive analytical effort and require complicated mathematical programming. A set of simple analysis and synthesis equations has been presented for broadside-coupled suspended substrate [7, 8], but it has a limited range of structural parameters. In practice, there is a strong need to analyze the broadside-coupled suspended substrate stripline with a wide range of structural parameters and better accuracy with the simple closed-form expression. This paper presents an accurate analytical expression for broadside-coupled suspended substrate stripline over a wider range of structural parameters. These closed-form expressions are developed by curve-fitting. Based on these closed-form expressions, the transmission characteristics of broadside suspended substrate stripline can easily be analyzed by calculations. A synthesis program can easily also be developed using a simple iteration technique, which will make this expression suitable for computer-aided design of such transmission lines and circuits.